Nanotechnology

PAPER

A monitorable and renewable pollution filter based on graphene nanoplatelets

IOP Publishing Nanotechnology
Nanotechnology 31 (2020) 075701 (10pp) https://doi.org/10.1088/1361-6528/ab5072

A monitorable and renewable pollution filter based on graphene nanoplatelets

L Ferrigno[1], A Cataldo[2], S Sibilia[1], A Maffucci[1,2] and S Bellucci[2]

[1] Department of Electrical and Information Engineering, University of Cassino and Southern Lazio, Via G. di Biasio 43, 03043, Cassino, Italy
[2] INFN-Laboratori Nazionali di Frascati, via E. Fermi 40, 00044 Frascati, Italy

E-mail: maffucci@unicas.it

Received 21 August 2019, revised 18 September 2019
Accepted for publication 23 October 2019
Published 14 November 2019

Abstract

This paper deals with the fabrication, modeling and experimental characterization of a monitorable and renewable graphene-based pollution filter. The main goal is to demonstrate a method to monitor the status of such a filter in real time during its operating phases: pollutant adsorption, saturation, and regeneration. The filter is realized by a disk of pressed graphene nanoplatelets. This is a low-cost type of graphene which has recently drawn great interest due to its potential use in large scale industrial production. Here the nanomaterial is obtained through the exfoliation method assisted by microwave irradiation, by exploiting the thermal expansion of commercial intercalated graphite, according to a low-cost and ecologically friendly procedure. The filter is used here to adsorb acetonitrile, a toxic water-soluble organic compound that is present in some industrial solvents and paints. The monitoring method is based on the interpretation of the time variation of the electrical impedance measured during filter operation. There are two main results of the paper: Firstly, the graphene filter is shown to be effective in adsorbing the above pollutant, with the additional feature of being fully renewable: all the pollutant can be removed from the filter without the need of costly physical or chemical processes. Secondly, monitoring of the time-evolution of the electrical impedance allows efficient detection of the different phases of the filter life cycle: clean, polluted, saturated and regenerated. This feature is of potential interest since it enables the predictive maintenance of such filters.

Keywords: graphene nanoplatelets, monitoring, pollution filter, impedance analysis, electrical characterization

(Some figures may appear in colour only in the online journal)

1. Introduction

Given their unique properties such as low density, large specific surface area, and outstanding electrochemical performance [1], graphene-based materials have been recently proposed for environmental applications like pollution filtering [2, 3]. An application of potentially great interest is water remediation, since nowadays water pollution by soluble toxic compounds is causing great concern and thus a huge world-wide effort has been devoted to assessing more and more efficient technological solutions for water cleaning. Graphene filters have been proven to clean water about ten times faster than current commercial filters [3] and to be effective in removing metal ions and organic compounds [4].

Nowadays, the most popular water remediation technology is that based on activated carbon (AC) filtration that still demonstrates the most convenient cost/effectiveness ratio among the available solutions [5]. Although this popular technology is effective to reduce contaminants such as some organic chemicals and heavy metals like lead [5], its main limitations are given by:

(i) limited range of pollutants adsorbed;
(ii) non-negligible impact of the fabrication process;
(iii) costly maintenance and limited filter regeneration.

Indeed, AC filters do not have good performance in removing metals or bacteria and viruses. Additionally, their fabrication process has a non-negligible environmental impact, being based on solid material (typically petroleum

coke or peanut shells) to be activated in steam at very high temperature (about 1260 °C). As for the maintenance, the status of the filter can be only predicted and its substitution scheduled on intervals indicated by the manufacturers, instead of being related to the actual status. Finally, these filters may be regenerated only if they have not adsorbed toxic compounds, otherwise they become a waste and need to be treated with care [5, 6].

Two main solutions to the above issues are under investigation: enhancing the capture capacity of AC filters by chemical modification; or moving to new materials like graphene or other carbon-related materials, whose advantages over AC are foreseen to influence the next generation of filtering technologies [7].

Filters made of graphene related materials are known to be able to provide solutions to the above issues (i)-(ii). Indeed, properties like the presence of delocalized electrons, the high surface area and the possibility of being functionalized, allow such filters to broaden the spectrum of adsorbed pollutants, including for instance microorganisms [7–14]. As for the impact, graphene materials like the nanoplatelets used in this paper may be fabricated with low-impact and environmentally friendly processes (like that indicated in this paper in section 2). In addition, such solutions are characterized by a relatively low quantity of materials to achieve a target capacity [7]. As for issue (iii), the results of this paper suggest a promising way to face this problem.

In more detail, graphene-based filters have been so far proposed in the form of synthetic graphene oxide, GO [8–11], of functionalized structures such as metallic nanomaterials grown on graphene sheets [12], of carbon nanotubes, CNTs [13] or in hybrid carbon nanotube-graphene arrangements [14]. In all cases, graphene filters exhibit high adsorbing capacities towards dyes, antibiotics and heavy metals [10–14]. In particular, heavy metal ions such as cobalt and cadmium were considered in [8], showing that GO has the highest adsorption capacity among those used so far. This is mainly due to its large surface area and the presence of different functional groups containing oxygen on the surface, which make each atom of this element available to chelate the metal ion. In addition, the presence of delocalized π-electrons allows a strong complexation through an acid-base interaction of Lewis, which obviously contributes to the adsorption of ions. Another important feature is related to the thermodynamic behavior: during absorption the values of standard enthalpy and of standard entropy variations are indeed positive, indicating the absorption of heat and the spontaneity of the adsorption, respectively. A final advantage of using graphene is that at higher temperatures absorption becomes more favorable [11].

Given this promising performance, the main reason for which the graphene filters are not yet available as commercial solutions is their fabrication cost [7]. Therefore, great effort is devoted to industrialize such solutions, assessing technologies with the capability to scale production to high rates and low sale costs, guaranteeing the requested levels of reproducibility and reliability. For instance, in [15] the industrially adaptable method of blade coating has been used to manufacture large graphene membranes. At present therefore the above-mentioned materials (GO membranes, functionalized sheets, etc) do not fully meet the requirements for a suitable industrial technology, hence alternative solutions are still being investigated.

This paper investigates filters made by from so-called graphene nano-platelets, GNPs [16], a material that combines large-scale production, low costs and excellent physical properties, compared to other commercial graphene-related-materials [17],

The main goal is to demonstrate a method able to monitor in real time the status of such a filter during its operating phases: pollutant adsorption, saturation, and regeneration. The method is based on a joint use of experiments and modeling.

To this aim, section 2 describes the filter fabrication (§ 2.1) and the proposed monitoring method, along with the experimental setup details (§ 2.2). The filter is fabricated with a cheap and reliable technique, exploiting the results of our previous work [18–20]. The proposed real-time monitoring method is based on the measurement of the filter electrical impedance during the adsorption of the pollutant. The main idea is that of exploiting the high sensitivity of the graphene electrical parameters to the presence of external atoms inside its lattice, such as carrier mobility [21], electrical conductivity [22], electrical permittivity and magnetic permeability [23]. Note that this is the same principle that is exploited to tailor the electrical properties of graphene by using intentional doping [24].

In section 3, the monitoring setup is studied in detail, through experiment assessment, circuital modeling and calibration procedure. Then it is used to demonstrate the feasibility of the proposed technique. Specifically, this work studies the adsorption of acetonitrile, a water-soluble organic compound with a triple bond, widely adopted in industrial processes.

2. Materials and methods

2.1. Filter preparation

In this paper, the pollution filter has been fabricated with pressed GNPs. Although this nano-flake powder may be fabricated in several different ways, such as spark plasma synthesis [25], promising techniques suitable for industrial production are the so-called ball-milling [16], microwave radiation [18, 19], or the recently-proposed wet-jet milling processes [26].

Here, the GNPs have been produced via microwave radiation, starting from a commercial low-cost graphite from Anthracite Industries, Inc., of asbury carbons. It is graphite intercalated with sulfates and nitrates, positioned between the various carbonaceous layers, prepared in an acid environment (pH between 1 and 6). The GNPs are obtained by a low-cost, environmentally friendly and industrially scalable procedure based on microwave irradiation, sonication and a final vacuum filtration, which we have formerly proposed in [18–20].

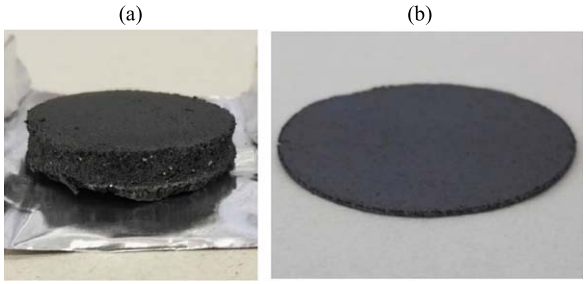

Figure 1. The GNP filter (a) before and (b) after being pressed.

Table 1. Dimensions (in mm) of the realized filter samples.

Sample #	1	2	3	4	5	6
Diameter	28.4	30.8	31.7	28.3	32.6	30.2
Thickness	0.6	0.6	0.6	0.6	0.7	0.7

Although pollution filters may be realized with many other types of graphene-related materials with different shapes and dimensions, a comparison of different materials is out of the scope of this paper, whose goal is to demonstrate a monitoring method. Note that the fabrication procedure implemented in our laboratory allows us to control the GNP transverse size and to obtain a few-layer graphene material (from 4 to 10 layers, see figure 1(b) in [27]). This feature is essential to provide to GNPs characteristics and properties almost comparable to those of the much more expensive graphene mono-layers, e.g., [18, 19]. The number of layers may be further reduced with deionized water during the exfoliation [28].

To fabricate the filter, the GNPs are further pressed at 700 N into a hollow cylinder, assuming the desired density (about $0.12\,\mathrm{g\,cm^{-3}}$) and shape (a disk with a diameter of about 3 cm, and a thickness of about 0.6 mm, figure 1). Six samples of the filters have been produced with the above technique, whose dimensions are given in table 1.

The SEM micrograph, reported in figure 2(a), shows the surface of pressed filter: the GNPs appear flattened and close each other to form a network in which are present pore-like hole. The contours and arrangement of the GNPs at the surface are depicted in figure 2(b) (by using the marker-controlled watershed segmentation technique, by Mathworks®). Note that the values of density and thickness are chosen to guarantee mechanical stability of the sample during the experiments.

A Raman characterization has been carried out on the produced GNPs, by means of a Renishaw® InVia Raman microscope, equipped with a 633 nm laser and an $1800\,\mathrm{l\,mm^{-1}}$ grating: in the stacked spectra, reported in figure 3, the G and 2D band are shown. Although the synthesis is carried out in atmosphere, any presence of oxidation are not detected, related to the D peak absence or at very low intensity. Furthermore, the wide range number of layers (4 to 10) is confirmed by the evolution of 2D peak [29].

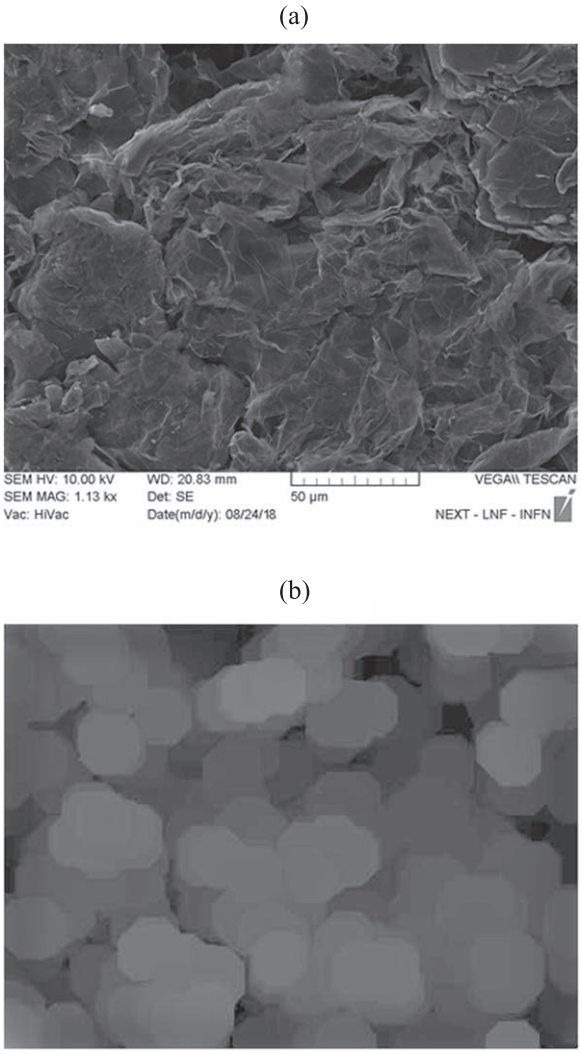

Figure 2. (a) SEM detail of the filter surface; (b) Marker-Controlled Watershed Segmentation of SEM image outlining the arrangement of GNPs at the filter surface.

Table 2. Results of the EDX analysis of the graphene nanoplatelets.

El.	Z	Series	Norm. C [wt%]	Atom. C [at%]	Err. (1 Sigma) [wt%]
C	6	K	85.40	89.62	9.72
O	8	K	11.09	8.73	1.67
Si	14	K	2.64	1.18	0.30
Na	11	K	0.60	0.33	0.08
S	16	L	0.22	0.09	0.31
N	7	K	0.05	0.04	0.05
		Total:	*100*	*100*	

Finally, an energy dispersive x-ray (EDX) analysis carried out on the GNPs highlighted a good level of purity of the material, as shown in table 2. The presence of O, S and N is due to the impurities coming from the fabrication process. In fact, as already mentioned, the exfoliation occurs by the suddenly evaporation of sulfates and nitrates, intercalated between graphene planes. Finally, Si and Na are impurities

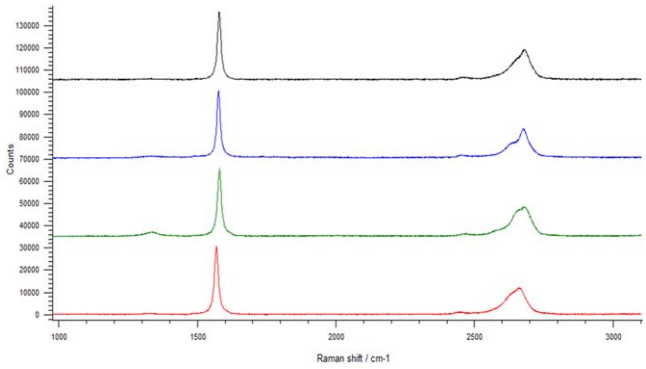

Figure 3. Stacked Raman spectra of the produced GNPs.

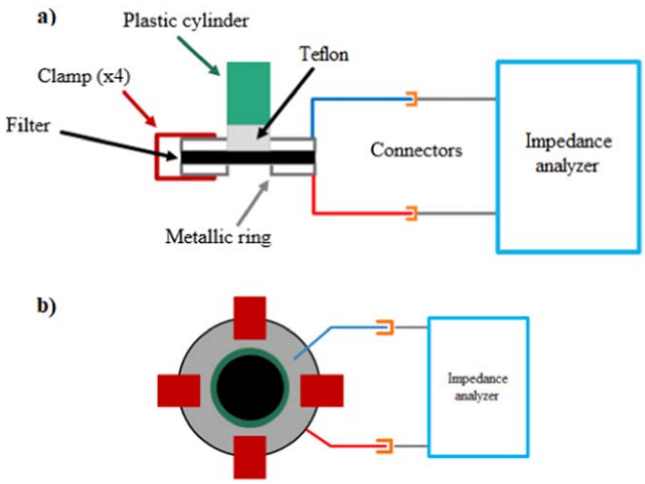

Figure 4 The proposed setup for the impedance measurement of the graphene filter: (a) side view; (b) top view.

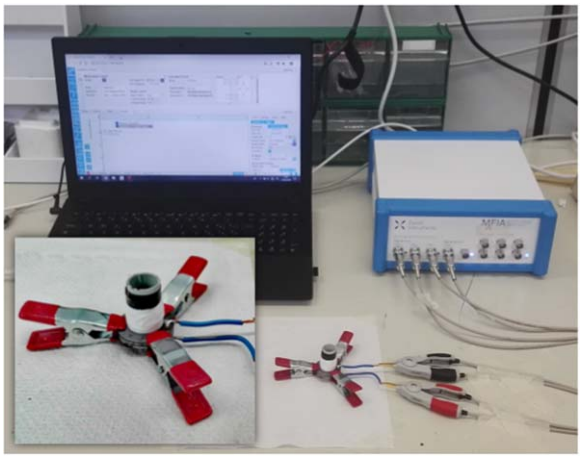

Figure 5. Setup for the measurement of the GNP filter impedance.

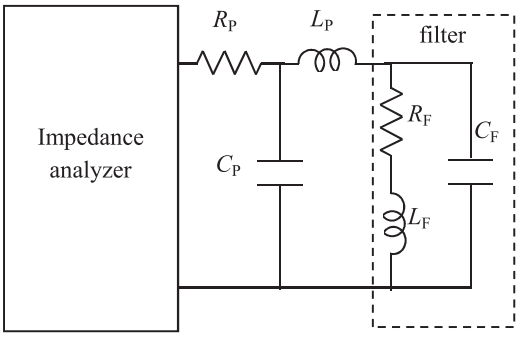

Figure 6. Equivalent circuit model for the experimental setup in figure 5.

coming from glassware or solvent during the sonication process.

2.2. Monitoring method: experimental setup and equivalent circuit model

As pointed out in the Introduction, the method proposed here is based on the joint use of the monitoring of the electrical impedance filter and of its interpretation based on an equivalent circuit model. The method is based on the well-known high sensitivity of the graphene electrical properties to the presence of external elements adsorbed in its lattice [21–23, 30], in this case the pollutant. To this end, the proposed system is monitoring the impedance in real time, during the filtering operation, without interfering with it.

The design and the realization of the proposed setup are reported in figures 4 and 5, respectively. The graphene filter is placed between two metal rings of the same dimensions, hold together by four insulated clamps. The two metal rings are then connected to an impedance analyzer. The polluted water flows through a hollow plastic cylinder located at the center of the filter. To avoid leakage, a Teflon tape (100% p.t.f.e.) is rolled around the cylinder's edge in contact with the upper metal ring.

The electrical impedance between the two rings is measured in real time as the process runs, by the impedance analyzer MFIA Precision LCR meter, Zurich Instruments (0–5 Mhz). The output data are then processed by a PC.

From the electrical point of view, the above setup may be modeled as in figure 6, where the cables, connectors, metal rings and all the parasitics between filter and impedance analyzer are taken into account by the cell R_p, L_p, and C_p. The filter is modeled as the series of a resistor R_F and an inductor L_F in parallel with a capacitor C_F, which are dependent on both geometrical properties (dimension, porosity, GNP aggregation characteristics,…) and physical ones (e.g., electrical conductivity σ and permittivity, ε, and magnetic permeability, μ).

Note that the instrument models the impedance as $Z_m = R_s + iX_s$, and hence the following relations hold with respect to the model given in figure 6:

$$R_S = \frac{R_F}{1 + \omega^2 C_F^2 \left(R_F^2 + \omega^2 L_F^2 - 2\frac{L_F}{C_F} \right)}, \qquad (1)$$

Table 3. Measured impedance before and after calibration.

	R_s (mΩ)	X_s (mΩ)
Before calibration	22.02	391.7
After calibration	−0.68	−0.05

$$X_S = \frac{\omega L_F\left(1 - R_F^2\frac{C_F}{L_F} - \omega^2 L_F C_F\right)}{1 + \omega^2 C_F^2\left(R_F^2 + \omega^2 L_F^2 - 2\frac{L_F}{C_F}\right)}. \quad (2)$$

A proper calibration procedure is then needed to completely remove the effects of all the impedances external to the filter (R_p, L_p, and C_p). To this end, in this paper a short-open (SO) calibration was used, with specific changes to be adopted in order to compensate the presence of the two metal rings. Indeed, the open circuit condition was here imposed by replacing the filter with an insulating disk made by three pieces of electrical tape. The short circuit was realized by interposing a copper plate between the rings, in contact with them. The effectiveness of the calibration is shown in table 3, which reports the measured impedance for the short circuit configuration before and after calibration: after the calibration the impedance is put to zero. The impedance has been measured at 100 kHz, which is the frequency chosen for all the experiments here, as explained later on.

The calibration is a key aspect in the proposed technique, since it improves the reproducibility of the measurements in presence of hand-made setups, lowering the uncertainties related to the filter/ring contacts actually realized for each single experiment. Indeed, it is well-known in literature that the metal/graphene contacts may strongly affect the performance of systems embedding conventional conductors and GNPs [30].

3. Results and discussion

3.1. Experiment description and setup assessment

The experiment proceeds as follows. After the initialization of the system, a controlled quantity (1 ml) of pollutant is manually dropped into the hollow cylinder by using a syringe, in a few seconds. The acetonitrile (Sigma Aldrich, ACS reagent ⩾99.5%, d = 0.786 g ml^{-1} at 25 °C) is adsorbed by the filter up to its saturation. Next, the pollutant spontaneously evaporates (being extremely volatile) leaving the filters completely clean. Note that acetonitrile in form of gas could, in principle, be recycled if the graphene filter were surrounded by a suitable kind of extractor hood. Figure 7 reports the time evolution of the measured impedance, after the calibration (hence they refer to the filter only).

The behavior of the resistance R_s and reactance X_s in figure 7 clearly show the phases of the experiment: during the adsorbing of the pollutant, the resistance increases, whereas the reactance decreases, changing its sign from positive (inductive) to negative (capacitive). The saturation is reached at the time instant when X_s reaches its minimum value. Next,

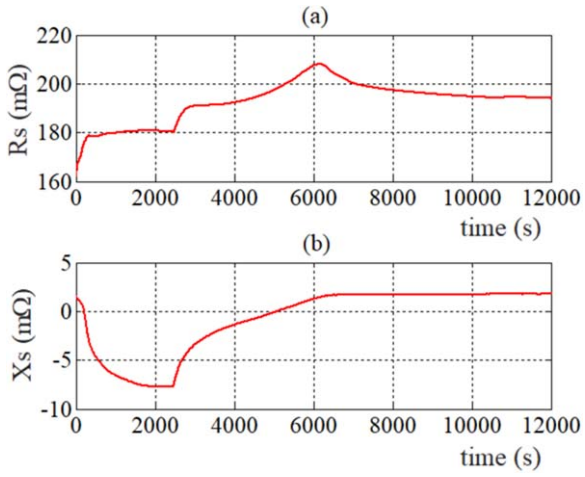

Figure 7. Time-domain evolution of the electrical parameters of the filter during adsorption and evaporation of the pollutant (sample #2).

Table 4. Weights of the filters before and after the experiment.

Sample #	1	2	3	4	5	6
Initial (g)	0.194	0.209	0.187	0.189	0.193	0.175
Final (g)	0.195	0.211	0.187	0.188	0.193	0.175

Table 5. Signal-to-noise ratio (3) measured for each filter sample.

Sample #	1	2	3	4	5	6
SNR (dB)	103.9	95.1	89.3	95.4	96.4	99.9

the pollutant changes phase from liquid to gas and starts evaporating. During this time, X_s recovers to its initial value, whereas R_s continues to increase up to a maximum and then it has a slight decrease. Its final value is not equal to the initial one. An explanation of this behavior is provided later in this section. Here we observe that the complete evaporation of the pollutant is confirmed by the weights of the filters, measured at the end of the experiments, which are the same as the initial ones, see table 4. When the filters are saturated by the pollutant their weights increase significantly (almost doubling), reaching values in the range between 0.37 g and 0.40 g.

By summarizing, the experimental results on this setup demonstrate that: (i) the GNP filter is able to adsorb the considered pollutant, up to a saturation point when it almost double its weight; (ii) the filter is self-cleaning, due to the evaporation of the pollutant; (iii) during the operation cycle, the impedance of the filter changes significantly its value.

To further investigate point (iii), it is useful to introduce a parameter that can quantitatively estimate these variations, the signal-to-noise ratio (SNR):

$$SNR = \frac{|\Delta X_w|_{\max}}{|\Delta X_{wo}|_{\max}}, \quad (3)$$

defined as the ratio between the amplitude dynamics of the reactance X measured with pollutant (subscript 'w') or without it (subscript 'wo'). These variations have been evaluated

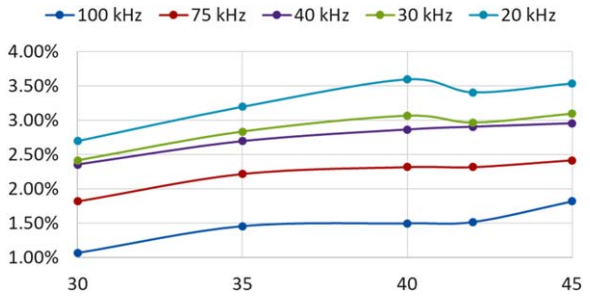

Figure 8. Sensitivity of the reactance to the environment (temperature) for different operating frequencies. Variations are estimated respect to the 25 °C reference temperature.

in time intervals of equal duration, which corresponds for each sample to the time required to come to the saturation, in presence of the pollutant. Table 5 reports the SNR measured for each sample, demonstrating a very high sensitivity of the proposed method, being such values no less than 89 dB.

A final step in the setup assessment is related to the choice of the frequency. Here the frequency value has been chosen in order to minimize the variation of the measured impedance (in particular the reactance) with the environmental conditions. In figure 8 it is reported the percentage variation of the reactance measured for a clean filter, with varying values of temperature respect to the 25 °C considered as reference. Based on this result, in the following we have chosen 100 kHz as the operating frequency since it provides lower variations in absolute values and shows a stable zone between 35 °C and 40 °C.

3.2. Characterization results and interpretation

To check the reproducibility and repeatability of the proposed monitoring method, in the first experiment all the six filters have been subject to a complete cycle as the one described in figure 7. In particular, they have been completely saturated, by putting a large amount of pollutant greater than that the filter is able to retain. In figures 9 and 10 it is shown the time evolution of the measured resistance and reactance, for three samples (a similar behavior is observed for the others).

The results in figure 10 clearly show that for all the samples the reactance X_s exhibits the same qualitative behavior. On the other hand, from figure 9 it can be observed that the behavior of the resistance R_s does not show the same degree of reproducibility, although some common features may be observed: (i) it is increasing during the adsorption, reaching an almost flat value; (ii) it increases again from the instant when the pollutant changes its phase and starts evaporating, reaching its maximum at the complete evaporation; (iii) after then, it has a slight decreases.

From sample to sample, the variability of the initial values of the resistance and reactance is mainly related to the non-uniformity of the distribution of the GNPs, rather than to the filter dimensions, whose variations are negligible (table 1). Indeed, the randomicity in the GNP sizes and distribution in the filter gives rise, for instance, to different current paths (see figure 11(a)) and hence to a different value

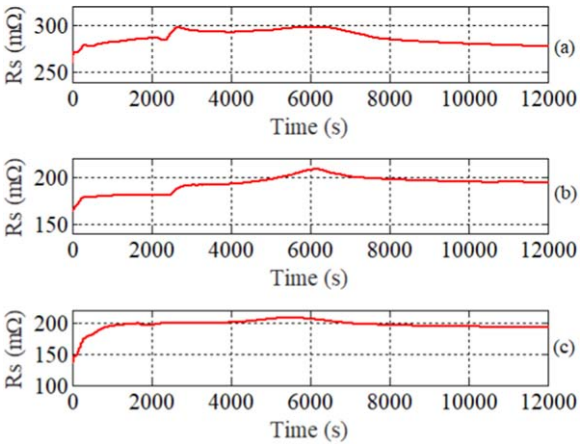

Figure 9. Time-domain evolution of the electrical resistance of the filter: (a) sample #1; (b) sample #2; (c) sample #4.

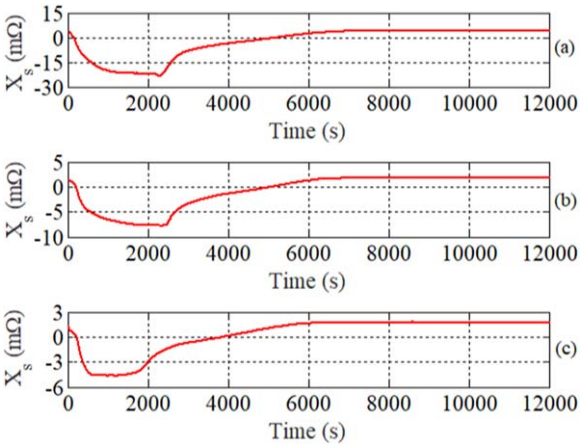

Figure 10. Time-domain evolution of the electrical reactance of the filter: (a) sample #1; (b) sample #2; (c) sample #4.

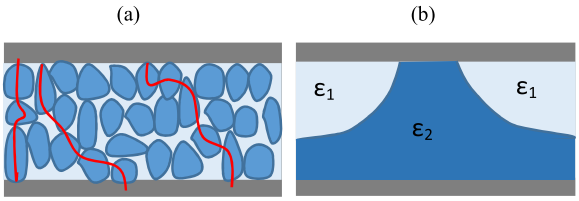

Figure 11. Cross-section of the circular filter connected to the metal plates: (a) the non-uniform distribution of GNPs induces random current paths; (b) a possible profile of the equivalent permittivity after adsorbing of the pollutant, with two equivalent homogeneous permittivity values for the two phases (clean and saturated filter).

of R_F and L_F from sample to sample. Similar considerations hold for the effect on the capacitance *cf*

The behavior of the impedance in figures 9 and 10 may be reproduced by relating the equivalent circuit parameters in figure 6 to the physical properties of the GNP filter. Indeed, the resistance R_F and capacitance C_F may be modeled by:

$$C_F(t) = \frac{\varepsilon_r(t)\varepsilon_0 S}{h}, \quad R_F(t) = \frac{S}{\sigma(t)h}, \tag{4}$$

being ε_0 the vacuum space permittivity and S and h the GNP disk area and thickness, respectively. As for the inductance

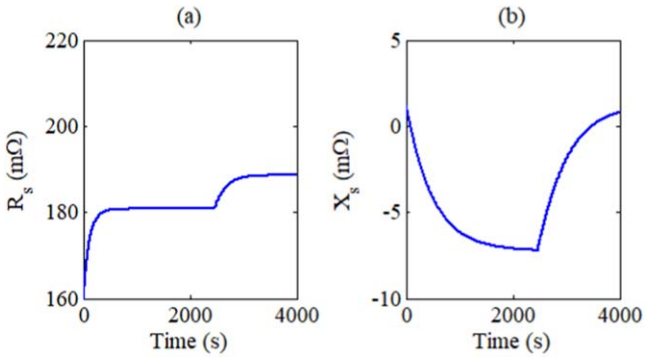

Figure 12. Simulated values of the resistance *Rs* and reactance *Xs*, obtained with model (1)–(6) for the sample #2.

L_F, its value can be estimated from the initial value of the reactance, as pointed out later.

In (3) we have used equivalent homogeneous permittivity, $\varepsilon_r(t)$, and conductivity, $\sigma(t)$, to easily describe the non-uniform material given by the GNP assembly and the pollutant. These effective parameters have been here modeled following the relation between electrical parameters and doping suggested by the literature (e.g., [21–23, 30]). Indeed, as the pollutant is adsorbed, we can assume the electrical conductivity σ to decrease, the relative electrical permittivity ε_r to increase and the relative magnetic permeability μ_r to be almost insensitive, since the dopant has no magnetic properties. Let us indicate with ε_1 and ε_2 (σ_1 and σ_2) the equivalent homogeneous permittivity (conductivity) of the clean and saturated filter, respectively. These values may differ not only from sample to sample (due, for instance, to the different porosity), but also from experiment to experiment on the same sample, since the penetration of the pollutant inside the filter may lead to different spatial profiles, as for instance in figure 11(b).

Let us assume that the diffusion follows a simple time exponential law, hence in each time interval (t_1, t_2), we can model ε_r and σ as follows:

$$\varepsilon_r(t) = \varepsilon_{r1} + (\varepsilon_{r2} - \varepsilon_{r1})(1 - \exp(-(t - t_1)/\tau_\varepsilon)), \quad (5)$$

$$\sigma(t) = \sigma_1 + (\sigma_2 - \sigma_1)(1 - \exp(-(t - t_1)/\tau_\sigma)). \quad (6)$$

The final goal of this modeling analysis is that of providing a physical explanation of the observed behavior of both the real and imaginary parts of the impedance. To this end, in the following the model parameters (4)–(5) are identified by matching the experimental results, since they are related to the measured impedance through (1) and (2), after applying (3). More generally, however, the equivalent homogeneous parameters may be found by applying some of the techniques proposed, for instance, to homogenize nanocomposites and mixtures, such as those based on Maxwell-Garnett [31] or Brugemann formalisms [32]. Hybrid homogenization techniques based on the joint use of measurements and modeling are also available, like that presented in [33].

The model has been applied to the sample #2 providing the results plotted in figure 12, in good agreement with the measurement results (see figure 7). Two time intervals have been considered for the conductivity and permittivity model (4)–(5): from 0 to 2460 s and from 2460 s to 4000 s. The identified model parameters are given in table 6. The inductance was assumed to be $L_F = 2$ nH, which corresponds to the value that would provide the initial value of the reactance X_S when neglecting the capacitance. This approximation does not introduce significant errors, since the waveforms in figure 12 are slightly sensitive to L_F.

The values of conductivity are in the expected order of magnitude: for a similar arrangement (an electrical contact made by layered GNPs) the low-frequency conductivity has been found to be in the order of some S/m [29]. However in the configuration studied in [33] the current flows parallel to the GNP surface, whereas in this case the flakes are randomly orientated in the bulk GNP disk, therefore the currents may also flow perpendicularly. In this case, the equivalent conductivity decreases since the conduction is mainly associated to the inter-layer or inter-flake tunneling, rather than to the electrical contact between them. Also the identified permittivity values are compatible to those that can be found in literature for GNP assembly, such as nanocomposites [34, 35].

The model is able to reproduce the measured values assuming that: (i) during adsorption (time interval: 0–2460 s) the conductivity σ decreases and the permittivity ε_r increases; (ii) during the first part of the evaporation (time interval: 2460–4000 s) ε_r decreases again whereas σ keeps on decreasing. In addition, in the two intervals the time constants for ε_r are the same, whereas for σ are different in the two intervals, suggesting that a new phenomenon occur in the second time interval.

The above results can be explained by observing that the presence of the pollutant (first interval) has a different impact on the σ and ε_r. Since the current flows perpendicularly to the GNP surfaces, the pollutant molecules lower the conductivity mainly when they intercalate between layer and layer (inside a single GNP) or between GNP and GNP. In this way they reduce the effectiveness of the contacts or of the tunneling (which are the two main inter-layer conduction mechanism). As for ε_r, the presence of the pollutant molecule has an impact on the electric field by altering the local reaction field. The electric field, however, is slightly sensitive to the reciprocal position of the GNP flakes. After the filter has saturated, the acetonitrile changes its phase from liquid to gas. This changes locally the pressure resulting in an increased distance between layers and layers of the same or different GNPs. As pointed out before, this will make more difficult the current flow, but will not have any effect on the electrical field. This 'local expansion' continues during the phase change leading the resistance to a maximum (see figures 7 and 9). After this time, the conductivity slightly increases (and so R_s slightly decreases), due to GNP assessment (probably related to the action of the Van der Waals forces). This interpretation is also confirmed by the fact that the initial value of the resistance of the filter is increasing from run to run, when using the same sample for multiple cycles (as in the second experiment later on).

Table 6. Values of the circuital model parameters for simulating the impedance of the sample #2 in figure 12.

	ε_{r1}	ε_{r2}	σ_1 (S m^{-1})	σ_2 (S m^{-1})	τ_ε (s)	τ_σ (s)
(0–2460) s	10	1200	0.160	0.141	500	100
(2460–4000)s	1200	10	0.141	0.135	500	200

3.3. Additional markers and repeatability test

We have so far observed that the time-domain reactance exhibits the same features in all the samples, although from samples to samples, the initial, final and the saturation values are different, as well as the time at which the saturation is reached. By checking its variations, it is then possible to monitor the status of the filter in real time.

Note that, although the absolute value of the resistance is apparently of poor utility, an interesting property arise when considering its variation DR_s, defined at any generic time instant t_n as follows:

$$DR_S(t_n) = R_S(t_n) - R_S(t_{n-1}), \tag{7}$$

Figure 13 compares the time evolution of X_s and DR_s for sample #1. In detail, the DR_s curve shows two 'pulses', highlighted in the boxes, which are temporally located in two main instants of the experiment. The first one occurs when X_s changes its behavior, being mostly capacitive. The second one is when X_s changes again its derivative going again towards an inductive behavior. These two instants can be considered as two milestones of the experiments. In detail, the first point is the time the filter senses the presence of the pollutant and becomes retaining it. The second point is the starting time of the phase change and of the evaporation of the pollutant, namely the phase in which the quantity of pollutant decreases and the filter goes toward its nominal weight. As a conclusion, the variation DR_s can be considered as a 'marker' of the filter state: its peak values occur at the time instants when the X_s parameter variation has to be analyzed. In addition, the time interval between these two peaks provides the duration of adsorbing process. Finally, as it happens for *Xs*, also DR_s exhibits the same values at the beginning and at the end of the experiments.

It would be useful to have a further marker to indicate the time when the filter is completely clean after evaporation. This can be obtained by checking the variability of the DR_s curve, by evaluating the standard deviation, s_{DRs}. In figure 14 this quantity has been evaluated on a slide window of 50 samples. It is clearly observed that at the end of the evaporation process (after a time of 10^4 s) the overall variability deeply reduces with respect to the filter activation zone (between 200 s and 10^4).

Summarizing, the variations of R_s provides the markers to the main time instants of the filter cycle: the peaks of DR_s indicate the start and the end of the adsorption, whereas the reduction of the standard deviation, s_{DRs} indicates that the filter is completely clean.

This result has been confirmed by studying all the other filters: for instance, figures 15 and 16 show the behavior of X_s and DR_s for the samples #2 and #3, respectively. In addition, figure 17 describes the variability of DR_s for the sample #3. Once again, there is a difference between the minimum variability in the activation zone of the filter (e.g. presence of pollutant) and the typical variability in the no-activation zone (e.g. absence of pollutant) even if in this case the difference is smaller.

Finally, a second experiment has been carried out to assess the repeatability of the considered setup. Specifically, three consecutive tests have been executed on the same sample, namely sample #1. Results for the X_s and DR_s

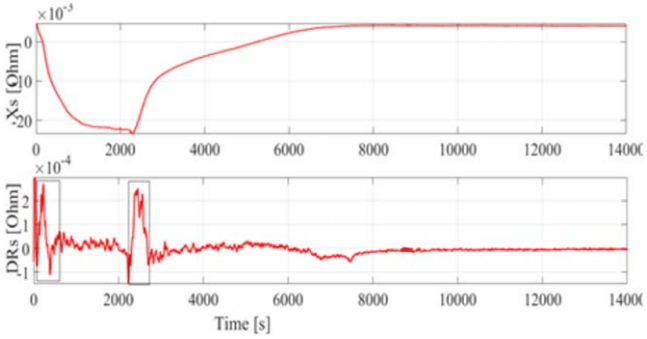

Figure 13. Time-domain evolution of *Xs* and DR_s during adsorption and evaporation of the pollutant (sample #1).

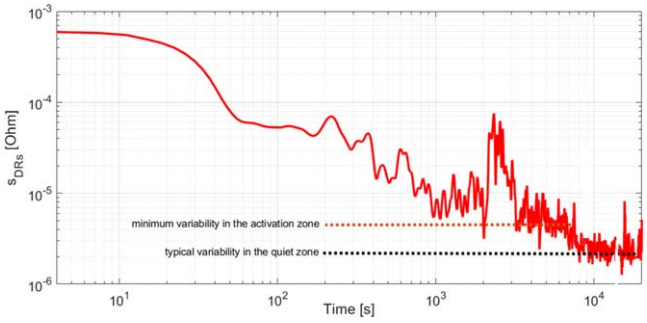

Figure 14. Time-domain evolution of the standard deviation of DR_s, calculated on a slide window of 50 samples during adsorption and evaporation of the pollutant (sample #1).

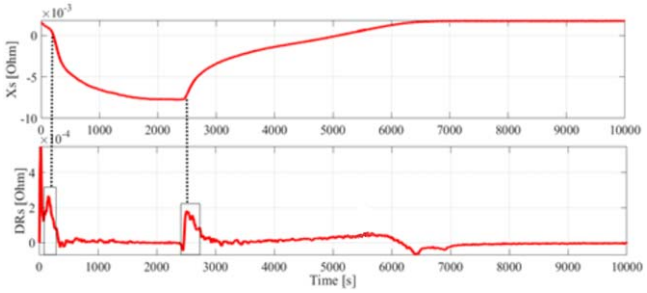

Figure 15. Time-domain evolution of *Xs* and DR_s during adsorption and evaporation of the pollutant (sample #2).

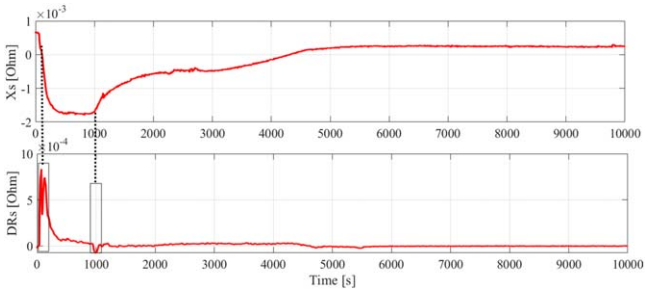

Figure 16. Time-domain evolution of *Xs* and DR_s during adsorption and evaporation of the pollutant (sample #3).

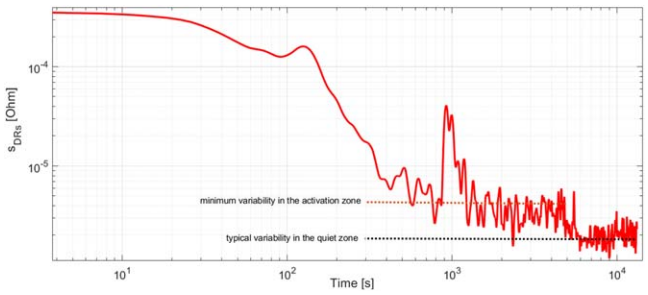

Figure 17. Time-domain evolution of the standard deviation of DRs, calculated on a slide window of 50 samples during adsorption and evaporation of the pollutant (sample #3).

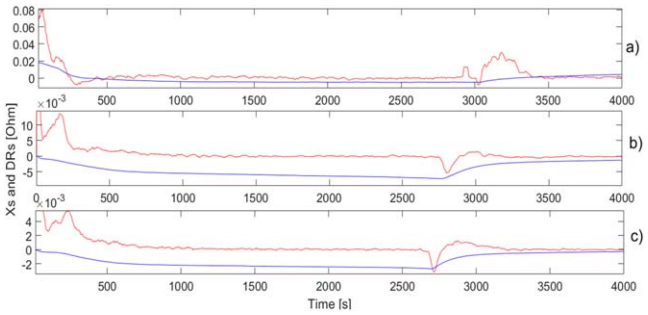

Figure 18. Time-domain evolution of X_s (blue line) and DR_s (red line) for three different runs of adsorption and evaporation involving the sample #1: (a) run #1; (b) run #2; (c) run #3.

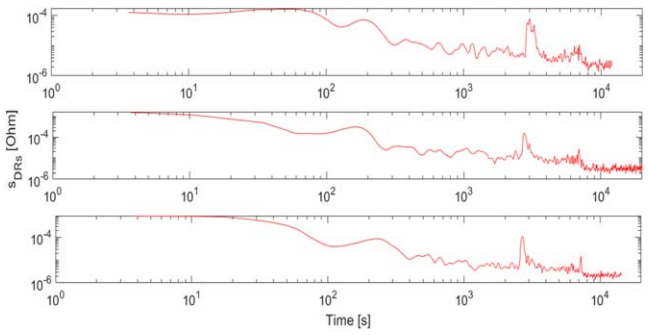

Figure 19. Time-domain evolution of the standard deviation of DR_s calculated on a slide window of 50 samples during adsorption and evaporation of the pollutant. Three different runs on sample #1 have been executed: (a) run #1; (b) run #2; (c) run #3.

parameters are reported in figure 18, while the variability of DR_s is reported in figure 19. Looking at all the results it is possible to confirm all the statements reported above. In detail, in all the considered tests there is a strictly relation between the X_s and DR_s behaviors that make DR_s a reliable marker of the pollutant sensing and evaporation phases and, once again, the analysis of the variability of DR_s shows information about the quiet state of the filter.

4. Conclusions

This paper has successfully assessed a method for monitoring in real time the status of a pollution filter realized by pressed graphene nanoplatelets (GNP), while adsorbing acetonitrile. The monitoring technique is based on the measurement of the electrical impedance of the filter, at the chosen frequency of 100 kHz (that optimizes the stability with respect to the environmental temperature).

The fabricated GNP filter has been shown: (i) to be able to adsorb the considered pollutant, up to a saturation point when it almost double its weight; (ii) to be self-regenerating due to the evaporation of the pollutant

The monitoring method has been shown to be reliable, given the high level of reproducibility and repeatability of its results, with a signal-to-noise ratio of about 90 dB. The imaginary part of the impedance (reactance) has been shown to follow a qualitative behavior that clearly indicates the time domain evolution of the filter life (clean, polluted, saturated and regenerated). In addition, the start and end times of each of those phases can be clearly determined by the markers that can be derived from the real part of the impedance (resistance).

The observed behavior of the impedance has been given a physical explanation by using a model which assumes an exponentially decreasing electrical conductivity and increasing permittivity as the pollutant is adsorbed by the filter.

The demonstration of the proposed method encourages further steps in view of assessing a potential industrial application of this idea, which can be of interest for instance for enabling predictive maintenance. With reference to the setup proposed here, an optimization step would be necessary, with reference to parameters that may strongly influence the performance, such as the GNP size or the GNP/electrode contact. In addition, other types of GNP or other graphene-related materials may be investigated and compared to the GNP adopted here, to check for instance the influence of the material specific features like the shape.

Acknowledgments

The work was partially supported by the project TERASSE, call H2020-MSCA-RISE 2018, Grant No. 823878, and by the project 'Smart Distributed Systems', Call MIUR (Italian Ministry of University) 'Dipartimenti di Eccellenza 2018-2022'.

We acknowledge Samuele Giovannetti for his support in the preparation and characterization of the filters.

ORCID iDs

L Ferrigno https://orcid.org/0000-0002-1724-5720
A Cataldo https://orcid.org/0000-0003-4662-9106
A Maffucci https://orcid.org/0000-0002-4992-9449
S Bellucci https://orcid.org/0000-0003-0326-6368

References

[1] Brownson D A *et al* 2014 *The handbook of Graphene Electrochemistry* (Berlin: Springer)
[2] Wu Y, Zhu J and Huang L 2019 A review of three-dimensional graphene-based materials: synthesis and applications to energy conversion/storage and environment *Carbon* **143** 610–40
[3] Huang H, Song Z and Wei N 2013 Ultrafast viscous water flow through nanostrand-channelled graphene oxide membranes *Nat. Commun.* **4** 2979
[4] Perreault F, De Faria A F and Elimelech M 2015 Environmental applications of graphene-based nanomaterials *Chem. Soc. Rev.* **44** 5861–96
[5] Cecen F and Aktas O 2011 *Activated Carbon for Water and Wastewater Treatment* (New York: Wiley)
[6] Chowdhury Z K *et al* 2013 *Activated Carbon: Solutions for Improving Water Quality* (Denver, CO: American Water Works Association)
[7] Sweetman M, May S, Mebberson N, Pendleton P, Vasilev K, Plush S and Hayball J 2017 Activated carbon, carbon nanotubes and graphene: materials and composites for advanced water purification *C Journal of Carbon Research* **3** p18
[8] Wang H *et al* 2013 Adsorption characteristics and behaviors of graphene oxide for Zn (II) removal from aqueous solution *Appl. Surface Sciences* **279** 432–40
[9] Nair R R, Wu H A and Jayaram P N 2012 Unimpeded permeation of water through helium-leak-tight graphene-based membranes *Science* **335** 442–4
[10] Joshi R K, Carbone P and Wang F C 2014 Precise and ultrafast molecular sieving through graphene oxide membranes *Science* **343** 752–4
[11] Zhao G, Li J, Ren X, Chen C and Wang X 2011 Few-layered graphene oxide nanosheets as superior sorbents for heavy metal ion pollution management *Environ. Sci. Technol.* **45** 10454–62
[12] Vadahanambi S, Lee S-H, Kim W-J and Oh I-K 2013 Arsenic removal from contaminated water using three-dimensional graphene-carbon nanotube-iron oxide nanostructures *Environ. Sci. Technol.* **47** 10510–7
[13] Yang S Y, Vecitis C D and Park H 2019 Electrocatalytic water treatment using carbon nanotube filters modified with metal oxides *Environmental Science and Pollution Research* **26** 1036–43
[14] Sui *et al* 2012 Green synthesis of Carbon nanotube-graphene hybrid aerogels and their use as versatile agents for water purification *J. Mater. Chem.* **22** 8767–71
[15] Akbari A *et al* 2016 Large-area graphene-based nanofiltration membranes by shear alignment of discotic nematic liquid crystals of graphene oxide *Nat. Commun.* **7** 10891
[16] Young R J, Kinloch I A, Gong L and Novoselov K S 2012 The mechanics of graphene nanocomposites: a review *Compos. Sci. Technol.* **72** 1459–76
[17] Kovtun A *et al* 2019 Benchmarking of graphene-based materials: real commercial products vs. ideal graphene *2D Mater.* **6** 025006
[18] Dabrowska A, Bellucci S, Cataldo A, Micciulla F and Huczko A 2014 Nanocomposites of epoxy resin with graphene nanoplates and exfoliated graphite: synthesis and electrical properties *Phys. Status Solidi* B **251** 2599–602
[19] Maffucci A, Micciulla F, Cataldo A, Miano G and Bellucci S 2016 Bottom-up realization and electrical characterization of a graphene-based device *Nanotechnology* **27** 095204
[20] Potenza M, Cataldo A, Bovesecchi G, Corasaniti S, Coppa P and Bellucci S 2017 Graphene nanoplatelets: thermal diffusivity and thermal conductivity by the flash method *AIP Adv.* **7** 075214
[21] Wei D, Liu Y, Wang Y, Zhang H, Huang L and Yu G 2009 Synthesis of N-doped graphene by chemical vapor deposition and its electrical properties *Nano Lett.* **9** 1752–8
[22] Kim K K *et al* 2010 Enhancing the conductivity of transparent graphene films via doping *Nanotechnology* **21** 285205
[23] Shahzad F *et al* 2015 Sulfur doped graphene/polystyrene nanocomposites for electromagnetic interference shielding *Compos. Struct.* **133** 1267–75
[24] Wang X, Sun G, Routh P, Kim D-H, Huang W and Chen P 2014 Heteroatom-doped graphene materials: syntheses, properties and applications *Chem. Soc. Rev.* **43** 7067–98
[25] Nieto A, Lahiri D and Agarwal A 2012 Synthesis and properties of bulk graphene nanoplatelets consolidated by spark plasma sintering *Carbon* **50** 4068–77
[26] Castillo A E D R *et al* 2018 High-yield production of 2D crystals by wet-jet milling *Material Horizons* **5** 809–904
[27] Volynets N I, Bychenok D S, Lyubimov A G, Kuzhir P P, Maksimenko S A, Baturkin S A, Klochkov A Y, Mastrucci M, Micciulla F and Bellucci S 2016 Shielding properties of composite materials based on epoxy resin with graphene nanoplates in the microwave frequency range *Tech. Phys. Lett.* **42** 1141
[28] Kim H-R, Lee S-H and Lee K-H 2018 Scalable production of large single-layered graphenes by microwave exfoliation 'in deionized water' *Carbon* **134** 431–8
[29] Ferrari A C *et al* Raman spectrum of graphene and graphene layers *Phys. Rev. Lett.* **97** 1874012006
[30] Bellucci S, Bovesecchi G, Cataldo A, Coppa P, Corasaniti S and Potenza M 2019 Transmittance and reflectance effects during thermal diffusivity measurements of GNP samples with the flash method *Materials* **12** 696
[31] Shanker B and Lakhtakia A 1993 Extended Maxwell Garnett model for chiral-in-chiral composites *J. Phys. D: Appl. Phys.* **26** 1746–58
[32] Mackay T G and Lakhtakia A 2015 Application of Bruggeman and Maxwell Garnett homogenization formalisms to random composite materials containing dimers *Waves Random Complex Medium* **25** 429–54
[33] Bellucci S, Maffucci A, Maksimenko S, Micciulla F, Migliore M D, Paddubskaya A, Pinchera D and Schettino F 2018 Electrical permittivity and conductivity of a graphene nanoplatelet contact in the microwave range *Materials* **11** 2519
[34] Bellucci S *et al* 2015 Broadband dielectric spectroscopy of composites filled with various carbon materials *IEEE Trans. Microw. Theory Tech.* **63** 2024–31
[35] Li Y C, Tjong S C and Li R K Y 2010 Electrical conductivity and dielectric response of poly(vinylidene fluoride)–graphite nanoplatelet composites *Synth. Met.* **160** 1912–9